

Article

# Carbon and Oxygen Isotopic Composition of Saline Lacustrine Dolomite Cements and Its Palaeoenvironmental Significance: A Case Study of Paleogene Shahejie Formation, Bohai Sea

Hailong Meng <sup>1,2</sup>, Zhengxiang Lv <sup>1,2,\*</sup>, Zhongmin Shen <sup>1,2,\*</sup> and Chenhao Xiong <sup>1,2</sup>

<sup>1</sup> State Key Laboratory of Oil-Gas Reservoirs Geology and Exploitation, Chengdu University of Technology, Chengdu 610059, China; menghailongcd@163.com (H.M.); treexch@126.com (C.X.)

<sup>2</sup> College of Energy Resources, Chengdu University of Technology, Chengdu 610059, China

\* Correspondence: lvzhengxiang13@cdut.cn (Z.L.); shenzhongmin@cdut.cn (Z.S.); Tel: +86-028-84079005

Received: 30 November 2018; Accepted: 21 December 2018; Published: 25 December 2018



**Abstract:** The dolomite reservoirs in the Paleogene Shahejie Formation in the Bozhong area of the Bohai Bay Basin contain a large amount of dolomite cement. Petrologic and mineralogic studies have shown that the dolomite cements can be divided into three types according to their occurrence: coating dolomite (CD), pore-lining dolomite (LD), and pore-filling dolomite (FD). The laser microsampling technique was used to analyze the C and O isotopes in the carbonate minerals. This method is an effective way to produce CO<sub>2</sub> gas from a particular carbonate structure in a thin section, and it has a spatial resolution of 20–50 μm and an optimal precision of approximately ±0.22σ for δ<sup>13</sup>C and δ<sup>18</sup>O in carbonate standard materials. The carbon and oxygen isotopic compositions and the oxygen isotopic geothermometer results showed that the dolomitization fluid is mainly low temperature fluid, the lake basin environment is relatively closed, and the salinity index Z value is greater than 120, which indicates the invasion of seawater. CD and early-stage LD crystals were mainly very fine crystals with faint cathodoluminescence, which indicates the early formation of diagenesis. The high temperatures of late-stage LD and FD measured by oxygen isotope thermometers indicates that they formed at a deeper depth. The dolomite cements in the study area may have formed in two stages: seepage-reflux dolomitization during the penecontemporaneous period and burial dolomitization.

**Keywords:** lacustrine carbonates; dolomite cements; Shahejie Formation; carbon-oxygen isotope; dolomitization; Bohai Bay Basin

## 1. Introduction

In both carbonate and clastic reservoirs, carbonate cementation, such as calcite or dolomite cementation, is often a key factor that affects reservoir quality [1–14]. The Eocene Shahejie Formation (hereafter referred to as “E<sub>2s</sub>”), which is located in the Shijiutuo Uplift in the middle of the Bohai Sea area, is a hydrocarbon reservoir with significant exploration potential [1,15–17]. The QHD29-2 oil field (Qinhuangdao, China), which has reserves of 100 million tons, was found in E<sub>2s</sub> [18]. Although the dolomite reservoir in E<sub>2s</sub> is nearly 4000 m deep, its residual primary porosity is still greater than 30% [19]. Most dolomite reservoirs form in marine environments [20–24]; most are intercrystalline pore reservoirs that formed by dolomitization [25,26]; and some formed as karst caves or are related to hydrothermal solution and the thermochemical sulfate reduction (TSR) [27–34]. However, the reservoir space of the dolomite reservoir in E<sub>2s</sub> is largely composed of primary pores, residual primary pores, and moldic pores [19,35]. The main characteristic of the dolomite reservoir in E<sub>2s</sub> is the development of a large amount of both syngenetic and authigenic dolomite cements [36]. The essential questions

regarding the dolomite cements in  $E_{2s}$  are as follows: (1) What are the origins of the dolomite? (2) How do the different types of dolomite differ from one another? (3) What effect does the type of dolomite have on the quality of the reservoir?

Based on an analysis of the petrological characteristics, mineral compositions, and carbon–oxygen isotope compositions of the dolomite cements, this paper discusses the genetic mechanisms of dolomite and the paleoenvironment during sedimentation. This study provides important guidance for reservoir prediction in the study area and also provides an opportunity to better understand lacustrine dolomite reservoirs, which mostly form under deep burial conditions.

## 2. Geological Background

The study area is located in the Eastern region of the Shijiutuo Horst in the middle of the Bohai Sea area, which borders the largest hydrocarbon-generating depression in the Bohai Sea area, the Bozhong Sag (Figure 1). The Bohai Bay Basin is located in a passive continental margin of the Pacific tectonic domain, and its Paleogene strata include the Kongdian Formation ( $E_{1-2k}$ ), the Shahejie Formation ( $E_{2s}$ ), and the Dongying Formation ( $E_{3d}$ ) [19,35–38]. The Cenozoic tectonic evolution can be divided into three stages. (1)  $E_{1-2k}$ – $E_{2s}^3$  was an extensional rift stage. Regional horizontal extension occurred, which was affected by mantle thermal activity, and an inherited boundary fracture developed in the depression and horst. (2)  $E_{2s}^2$ – $E_{3d}$  was a rift-subsidence stage. The fault activity decreased, and the basin was widely denuded during the Dongying sedimentary period. (3) The Neogene–Quaternary was the depression stage. Many secondary faults formed during this stage, forming a Y-shaped structure with the main fractures in the section (Figure 1) [18,39]. The Kongdian Formation in the study area consists of alluvial fan deposits that are mainly composed of interbedded mudstone and sandstone [40]. The Dongying Formation is mainly composed of mudstone, sandstone, and some interlayer siltstones, which are delta and lacustrine deposits [18].  $E_{2s}$  is mainly composed of fan delta deposits. However, at the front edge of the fan delta, carbonate platforms developed in the relatively high structures, where it was suitable for colonisation by gastropods and ostracods due to the shallow water, abundant sunlight, and minimal influence of terrigenous clasts [41–43]. The Paleogene  $E_{2s}$  contains several sets of bioclastic dolostones to the north and south of the Eastern margin of the Shijiutuo Uplift. This bioclastic dolostone is favorable for hydrocarbon reserves due to its high porosity and permeability [44] and is the main rock type of this study.

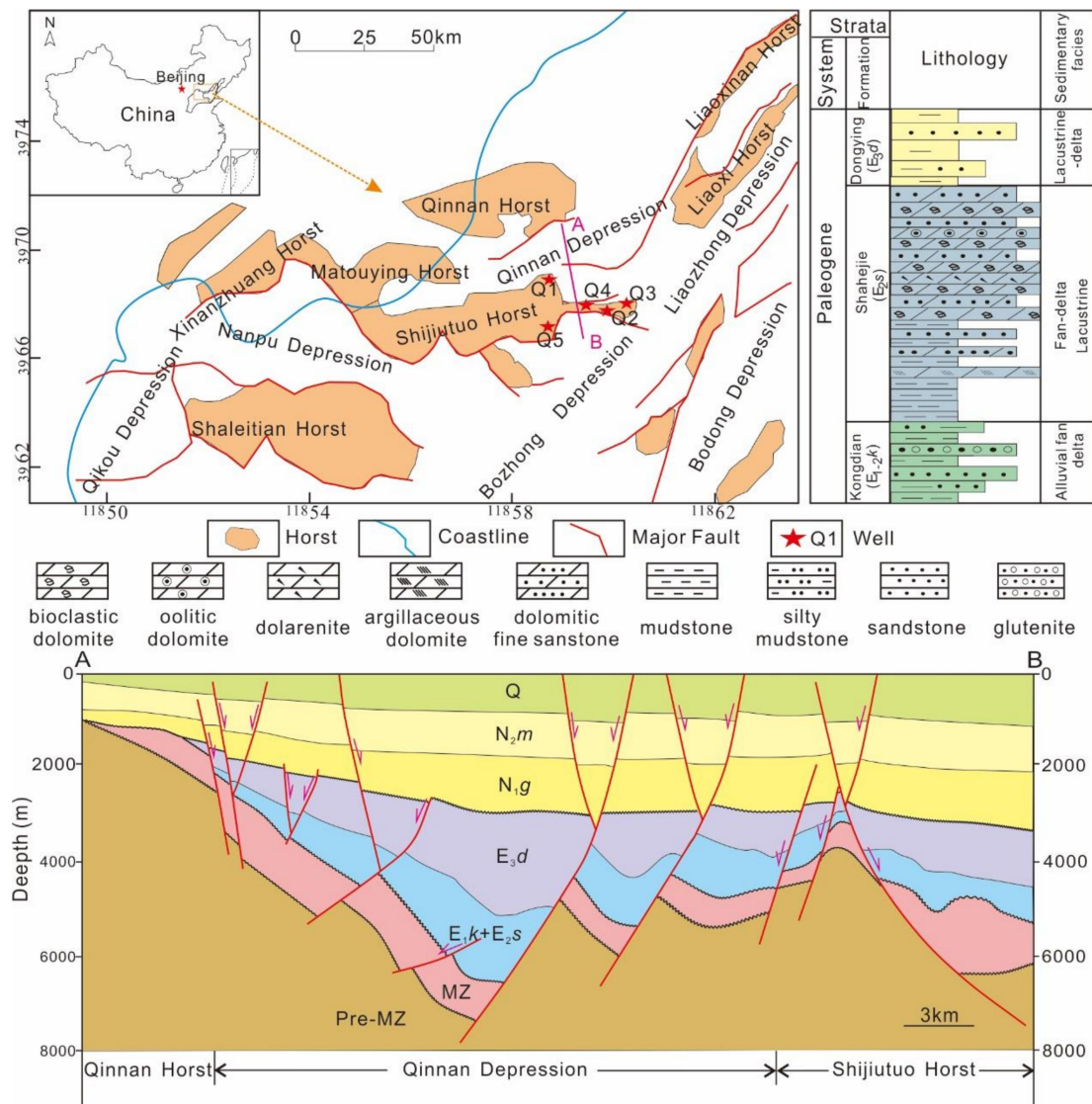


Figure 1. Map showing the structure of the study area and a lithological section of the Shahejie Formation.

### 3. Materials and Methods

One hundred and sixteen core samples were collected from the 5 recently drilled exploration wells in the Shijiutuo Uplift for physical analysis (including 88 carbonate samples and 28 mudstone samples). The samples were prepared as thin sections or ground to powders for petrographic, mineralogical, geochemical, and isotopic analyses. All of the thin sections were highly polished without coverslips and impregnated with blue epoxy to facilitate the identification of the pore space [45]. The sections were also stained with alizarin red S and potassium ferricyanide solutions to identify different types of carbonate cement (calcite stains red, whereas dolomite does not stain) [46].

Optical microscopy (Leica DM4500P) (Leica Microsystems Inc, Wetzlar, Germany) was used to observe the microscopic characteristics of the thin sections to determine their mineral compositions and diagenetic characteristics and to quantify their dolomite contents. A field-emission environmental scanning electron microscope (Quanta 250 FEG) (FEI, Hillsboro, OR, USA) was used to identify the minerals that could not be distinguished with a polarizing microscope. Furthermore, an energy spectrum analysis was used to determine the species of minerals that were difficult to identify due to their microcrystalline forms. This analysis was performed with acceleration voltages of 0.1 to 30 kV and working distances of 10 to 20 mm at a room temperature of 20 °C and a humidity of 51%.

Cathodoluminescence energy dispersive spectroscopy (EDS-X2072) can be used to differentiate between the original forms of authigenic dolomite; this analysis was performed using a vacuum level of 0.3 Pa, a beam voltage of 7.5 kV, and a beam current of 630–760  $\mu\text{A}$ . Fluid inclusions were analyzed by a Linkam THMS 600 heating–freezing stage in conjunction with an Olympus BX51 microscope, in which the measured temperatures ranged from  $-190$  to  $600$   $^{\circ}\text{C}$ , and the homogenization temperature error was  $<2$   $^{\circ}\text{C}$ . During the temperature analysis, the heating rate was initially controlled within  $10$   $^{\circ}\text{C}/\text{min}$  and then within  $1$   $^{\circ}\text{C}/\text{min}$  when approaching the critical phase transition.

Carbon and oxygen isotope ( $\delta^{13}\text{C}$  and  $\delta^{18}\text{O}$ ) compositions were determined by the laser microsampling technique, which is a useful tool that focuses a high-power laser beam onto a carbonate sample to liberate  $\text{CO}_2$  gas. The method uses a coaxial installation of a Nd:YAG laser (InnoLas, German) with a modified microscope. A high energy laser beam is focused on a thin slice sample in the vacuum sample box using the microscope's optical focusing system. The sample microarea is heated ( $>1500$   $^{\circ}\text{C}$ ), and the decomposed  $\text{CO}_2$  gas is purified by the purification line and then imported into the microinjection system of an isotopic ratio mass spectrometer (Finnigan MAT252) (Thermo Electron Corporation, Waltham, MA, USA). Compared to conventional methods, the microsampling technique can provide significant amounts of high resolution in situ data with a spatial resolution of  $20$ – $50$   $\mu\text{m}$  and an optimal precision of approximately  $\pm 0.22\sigma$  for both  $\delta^{13}\text{C}$  and  $\delta^{18}\text{O}$  in carbonate standard materials [47]. The stable carbon and oxygen isotope data are presented in  $\delta$  notation relative to the Vienna Pee Dee Belemnite (VPDB) standard.

Using a polarizing microscope to observe the authigenic dolomites in different regions, we marked the key areas where electron probe microanalysis was required (see Section 4.1 below). An EPMA 1720H electron probe microanalyzer (Shimadzu, Kyoto, Japan) was used to determine the chemical compositions of the different types of authigenic dolomite. The experimental conditions included an acceleration voltage of 15 KV, a beam spot size of  $30$   $\mu\text{m}$ , and a beam current of  $10$  nA.

To analyze the chemical compositions of the sedimentary environment, we conducted whole-rock analyses of 28 mudstone samples from  $E_2s$ . The macroelemental analysis of the mudstone was performed with a Shimadzu XRF-1700/1500 fluorescence spectrophotometer (Shimadzu, Kyoto, Japan).

## 4. Results

### 4.1. Petrophysical Characteristics

Based on petrographic observations, the bioclastic dolostone are mainly composed of bioclasts, terrigenous clasts, and intergranular micrite dolomite. The bioclasts are mainly gastropod and ostracoda fossils. Some of the fossil shells are replaced by dolomite, but the outline of the fossil remains intact (Figures 2a and 3e). Abundant authigenic dolomite has developed in the bioclastic dolostone of  $E_2s$  (including dolomitization after sedimentation and directly precipitated dolomite). The thin sections and SEM analysis revealed that the authigenic dolomite of  $E_2s$  occurs in three forms.

#### (1) Coating dolomite (CD)

This type of dolomite consists of very fine (mostly from  $10$  to  $15$   $\mu\text{m}$  crystals), generally planar-s to planar-e crystalline structures that cover bioclastic and oolitic carbonate particles and occur as micron-sized curved rhombic crystals. This type commonly forms a thin coating around grains and inside moldic pores (Figure 2a,b, Figures 3a and 4a,c). Most of the CD exhibited faint dull red luminescence under the cathodoluminoscope (Figure 3a,b).

#### (2) Pore-lining dolomite (LD)

This type of dolomite consists of fine (mostly from  $15$  to  $20$   $\mu\text{m}$  crystals), generally planar-s to planar-e dolomite crystals. This type of dolomite grows in the pore spaces between grains but does not develop at the points where the grains were in contact with each other (Figures 2c–e and 4a,b,d,e). In general, LD showed significantly enhanced cathodoluminescence, but different generations varied in their degree of luminescence. First-generation (LD-1), second-generation (LD-2)

and third-generation (LD-3) dolomites exhibited bright orange light, bright red light and dull red light, respectively (Figure 3c,d).

### (3) Pore-filling dolomite (FD)

This type of dolomite is found in the remaining pore space after the growth of pore-lining dolomite or the filling of moldic cavities. FD is composed of fine crystals (125 to 200  $\mu\text{m}$ ) containing a small proportion of finer planar-s to planar-e dolomite crystals (Figure 2e,f and Figure 4b,e). Most of the FD displayed luminescence of moderately bright orange light (Figure 3e,f).

E<sub>2</sub>s contains some oolites locally, which are generally superficial oolites. However, a few oolites with multiple concentric layers also developed (Figures 3g and 4f). In particular, those that have layers composed entirely of micrite dolomite have different cathodoluminescence in different layers (Figure 3g,h).

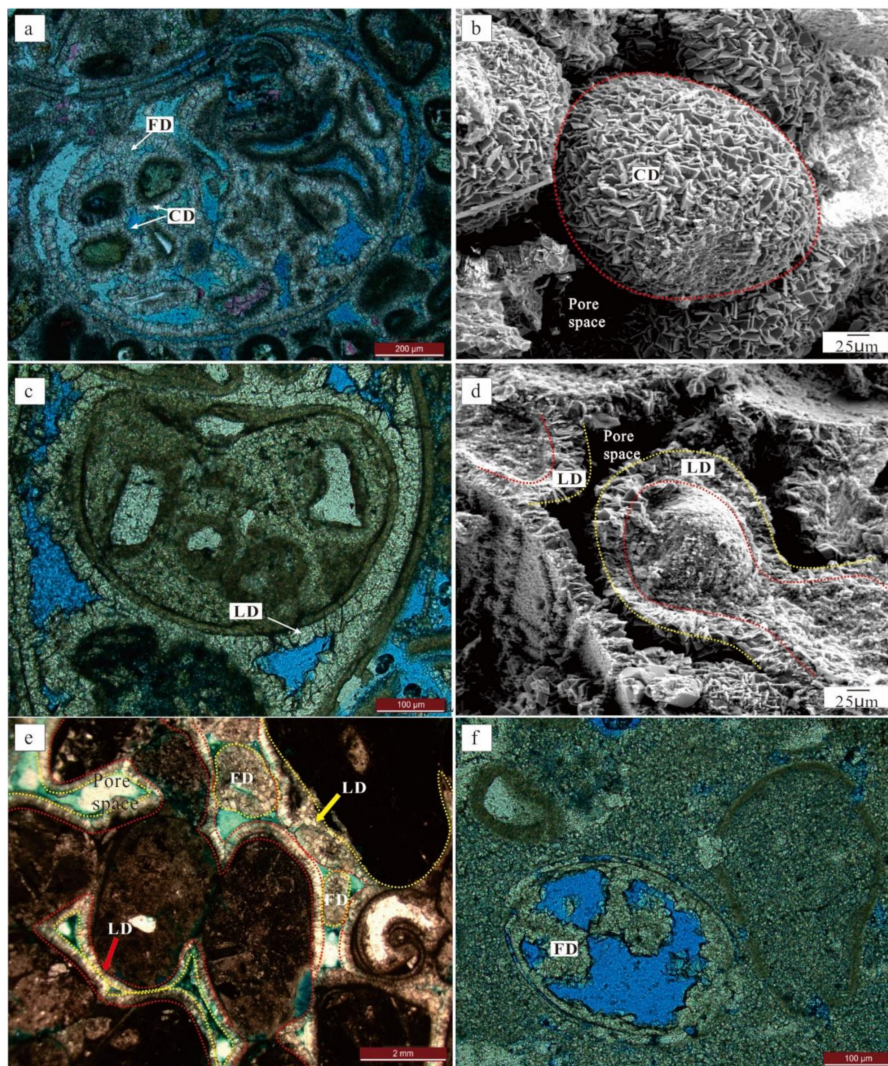


**Figure 2.** Optical thin sections and SEM images showing (a) crystalline coating dolomite (CD) wrapped around bioclastic grains in the form of isopachous cement and pore-filling dolomite (FD) in intergranular pores; (b) CD that clearly covers the surface of a peloid (energy spectroscopy: Mg: 3.67%, Ca: 5.13%, O: 49.68%); (c) Pore-lining dolomite (LD) developed around a moldic pore; (d) thin microcrystalline pore-lining dolomite (LD) that developed around various bioclasts (energy spectroscopy: Mg: 7.15%, Ca: 8.65%, O: 58.58%); (e) blade pore-lining dolomite (red arrow) with an isopachous rim that grew around intergranular pores, pendant pore-lining dolomite (yellow arrow) that is characterized by a distinct thickening of cement crusts beneath grains or under the roofs of intergranular and solution voids, and FD in intergranular pores; and (f) pore-filling dolomite (FD) in a moldic pore.

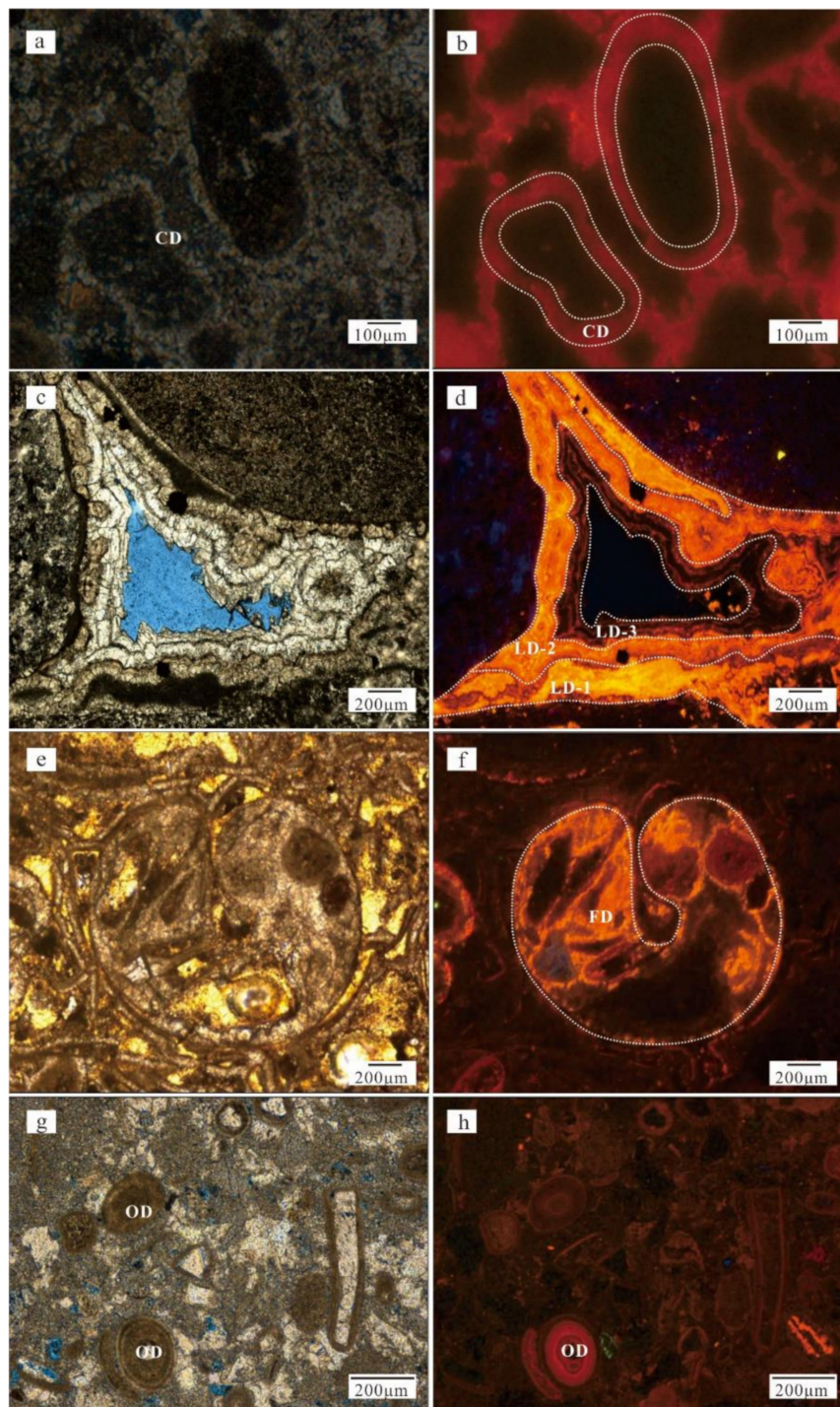


**Figure 3.** Cathodoluminescence (CL) images of authigenic dolomite in E<sub>2s</sub>: (a) thin isopachous microcrystalline coating dolomite (CD); (b) CL image of a, in which the CD exhibits faint–moderately dull red–orange red luminescence; (c) multigeneration interparticle pore-lining dolomite (LD) that developed in pellicular oolites; (d) CL image of c, in which the first-generation fine columnar dolomite exhibits bright orange luminescence (LD-1), the second-generation granular dolomite with a zonal structure exhibits bright red light (LD-2), and the third-generation granular dolomite exhibits dull red light (LD-3); (e) interparticle pore-filling dolomite (FD) filling a moldic cavity; and (f) CL image of e, in which the FD exhibits moderately bright orange luminescence; (g) oolitic dolomite (OD) with multiple concentric layers; and (h) CL image of g, in which the various cortical laminae of oolites have different degrees of cathodoluminescence.

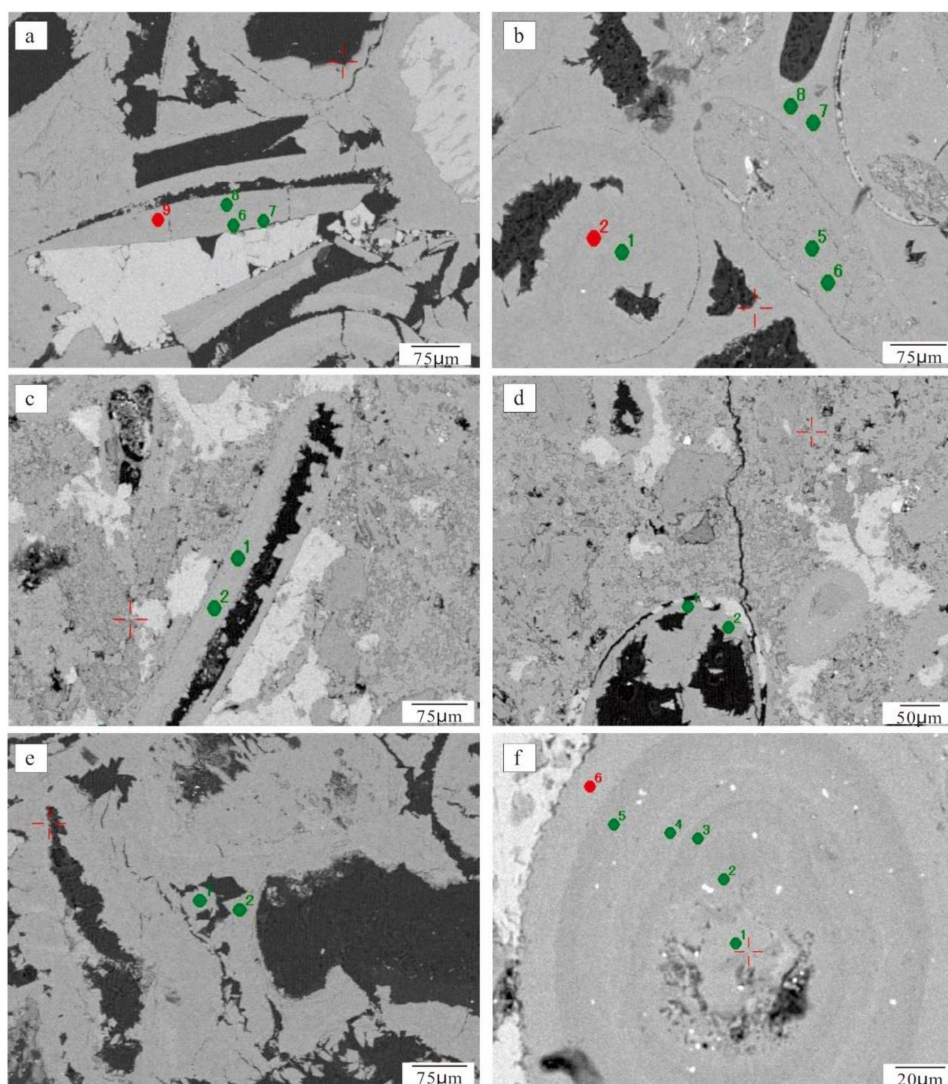


**Figure 4.** Optical backscattered electron microscope images of different types of dolomite: (a) microcrystalline coating dolomite (a-6, a-7) and crystalline dolomite on the inner wall of moldic pores (a-8, a-9); (b) pore-filling dolomite filling the moldic pores (b-1, b-2) and pore-lining dolomite developed around the residual intergranular primary pore (b-7, b-8); (c) microcrystalline coating dolomite wrapped around bioclastic grains (c-1, c-2); (d) crystalline dolomite on the inner wall of moldic pores (d-1); (e) pore-filling dolomite filling the residual intergranular primary pores (e-1) and pore-lining dolomite developed around the pore (e-2); (f) various cortical laminae of oolites (see analytical data in Table 3).

## 4.2. Geochemistry

### 4.2.1. Fluid Inclusion Microthermometry

In this paper, only one homogenization temperature data point, 27.8 °C, was obtained in the LD at a depth of 3382.1 m in well Q3, and no freezing point temperature data were obtained, which are mainly affected by factors such as small fluid inclusions, irregular shapes, and fuzzy boundaries between the inclusions and the host minerals.

### 4.2.2. Carbon and Oxygen Isotopes

The carbon and oxygen isotopic compositions of the CD in E<sub>2</sub>s (Table 1) showed that the  $\delta^{13}\text{C}$  values had a slightly broad range of 0.32‰ to 5.69‰ VPDB (mean 3‰ VPDB). The  $\delta^{18}\text{O}$  isotopic

values ranged from  $-5.82\text{‰}$  to  $-0.97\text{‰}$  VPDB (mean  $-3.4\text{‰}$  VPDB). The mean  $\delta^{13}\text{C}$  and  $\delta^{18}\text{O}$  values of the LD were  $2.89\text{‰}$  (from  $-0.42\text{‰}$  to  $5.41\text{‰}$  VPDB) and  $-4.53\text{‰}$  (from  $-9.35\text{‰}$  to  $-0.76\text{‰}$  VPDB), respectively. The  $\delta^{13}\text{C}$  values of the FD ranged from  $-0.51\text{‰}$  to  $4.08\text{‰}$  VPDB with an average value of  $1.46\text{‰}$  VPDB, whereas there was a wide range of  $\delta^{18}\text{O}$  isotopic values from  $-9.34\text{‰}$  to  $-2.27\text{‰}$  VPDB (mean of  $-5.59\text{‰}$  VPDB). Previous studies have suggested that the  $\delta^{13}\text{C}$  values of typical lacustrine carbonate rocks range  $-2\text{‰}$  to  $6\text{‰}$  and that the  $\delta^{18}\text{O}$  values vary from  $-8\text{‰}$  to  $-4\text{‰}$  [17,48,49]. The comparison showed that the carbon isotope compositions in the study area generally conform to the characteristics of typical lacustrine carbonate rocks, but the oxygen isotope compositions have an obvious positive deviation.

**Table 1.** Carbon and oxygen isotope data of different types of dolomite.

Well	Depth (m)	Type	$\delta^{13}\text{C}_{\text{PDB}}$ (‰)	$\delta^{18}\text{O}_{\text{PDB}}$ (‰)	Paleo Temperature (°C)	Salinity Index Z	Salinity S
Q3	3376.5	CD	0.32	-5.82	124.3	125.1	28.9
Q2	3762.6	CD	5.69	-0.97	88.4	138.5	33.8
Q3	3382.1	LD	4.7	-0.76	87	136.5	34.0
Q3	3375.06	LD	1.88	-4.01	110.4	129.2	30.7
Q3	3375.65	LD	-0.42	-9.35	153.4	121.8	25.4
Q2	3762.6	LD	5.41	-3.99	110.2	136.4	30.8
Q3	3378.92	FD	0.56	-2.27	97.6	127.3	32.5
Q3	3377.34	FD	1.78	-2.8	101.4	129.6	32.0
Q3	3380.25	FD	2.02	-4.97	117.7	129.0	29.8
Q3	3341.25	FD	2.67	-6.36	128.6	129.6	28.4
Q3	3376.65	FD	0.65	-5.64	122.9	125.8	29.1
Q3	3375.06	FD	0.15	-6.24	127.7	124.5	28.5
Q3	3341.78	FD	2.67	-6.36	128.6	129.6	28.4
Q3	3382.1	FD	-0.51	-8.73	148.1	121.9	26.0
Q3	3384.9	FD	0.53	-9.34	153.3	123.7	25.4
Q2	3762.6	FD	4	-3.16	104.1	133.9	31.6

#### 4.2.3. Calcium and Magnesium Compositional Characteristics

In the mudstone samples from E<sub>2</sub>s, the MgO contents ranged from 0.64% to 4.68%, and the Mg<sup>2+</sup>/Ca<sup>2+</sup> (molar) contents ranged from 0.18 to 4.84 (mean of 2.12; n = 28), indicating Mg<sup>2+</sup>-rich characteristics (Table 2). The analysis of the compositions of different circular oolitic layers revealed that the mean MgO and CaO contents of the inner layers were 36.92% and 60.1%, respectively, which were higher than those of the outer layers. However, FeO exhibited the opposite distribution, with the outermost layer having a higher content than the inner layers. The MgO contents of different dolomites showed that the LD had the maximum value (mean of 42.24%; n = 9), followed by the CD (mean of 38.15%; n = 4), whereas that of the FD was relatively low (mean of 37.43%; n = 4) (Table 3 and Figure 4f).

**Table 2.** Macroelemental compositions of mudstone in E<sub>2</sub>s.

Well	Depth	SiO <sub>2</sub> %	Al <sub>2</sub> O <sub>3</sub> %	CaO %	MgO %	Fe <sub>2</sub> O <sub>3</sub> %	K <sub>2</sub> O %	Na <sub>2</sub> O %	Mg <sup>2+</sup> /Ca <sup>2+</sup> Molar
Q5	3224.9	59.72	17.58	0.782	2.37	5.76	3.89	1.88	4.24
Q5	2915	61.32	15.4	0.738	2.07	6.48	3.25	1.85	3.93
Q5	2945	60.02	15.44	1.93	1.78	6.19	3.21	1.9	1.29
Q5	3005	57.26	16.51	0.867	2	6.99	3.33	1.91	3.23
Q5	3045	56.23	16.8	0.714	2.05	7.34	3.19	1.73	4.02
Q5	3095	57.2	16.68	0.723	2	6.68	4.03	1.36	3.87
Q5	3135	55.1	16.52	0.608	2.02	7.19	4.38	1.55	4.65
Q5	3175	52.93	15.56	1.51	2	7.73	4.68	1.67	1.85
Q5	3315	60.51	14.39	2.52	1.74	4.79	4.4	3.11	0.97
Q5	3345	54.42	13.17	4.38	2.82	5.08	4.39	2.48	0.90

Table 2. Cont.

Well	Depth	SiO <sub>2</sub> %	Al <sub>2</sub> O <sub>3</sub> %	CaO %	MgO %	Fe <sub>2</sub> O <sub>3</sub> %	K <sub>2</sub> O %	Na <sub>2</sub> O %	Mg <sup>2+</sup> /Ca <sup>2+</sup> Molar
Q5	3405	40.24	10.12	14.7	1.9	5	2.96	0.783	0.18
Q5	3440	51.66	11.04	5.38	1.72	5.43	3.58	1.23	0.45
Q4	3452.4	62.27	15.62	0.8	2.15	5.04	4.63	0.634	3.76
Q4	3452.5	60.75	15.22	1.14	2.05	6.29	4.65	0.58	2.52
Q4	3452.8	59.73	15.08	1.4	2.22	6.56	4.26	0.625	2.22
Q4	3453.3	61.83	15.24	2.51	2.01	4	3.4	0.571	1.12
Q4	3453.4	67.9	16.13	0.872	0.968	2.18	3.78	0.89	1.55
Q4	3453.7	73.53	11.22	2.04	1.01	1.92	3.73	0.541	0.69
Q4	3454.9	64.78	11.13	4.45	2.21	3.31	3.49	0.433	0.70
Q4	3455.7	65.66	12.57	3.2	1.73	3.99	3.5	0.492	0.76
Q1	3425	62.92	13.26	1.26	0.635	4.24	9.11	0.944	0.71
Q1	3145	54.23	16.92	0.853	2.18	7.07	4.12	1.43	3.58
Q1	3195	54.49	16.41	0.605	2.09	6.99	4.15	1.63	4.84
Q1	3250	50.12	14.62	6.08	2.02	6.56	3.38	1.24	0.47
Q1	3385	56.71	11.88	5.5	3.51	3.69	5.78	0.843	0.89
Q1	3590	43.03	13.2	2.24	4.68	12.13	3.69	1.58	2.93
Q1	3650	56.5	13.06	1.51	1.8	5.31	4.21	1.33	1.67
Q1	3680	57.97	13.5	2.46	2.19	6.36	4.18	1.22	1.25

**Table 3.** Results of the geochemical analyses of different occurrences of dolomite.

Well	Depth (m)	Photo No.	Point No.	Type	Na2O %	SiO2 %	MnO %	MgO %	SrO %	FeO %	K2O %	CoO %	CaO %	BaO %	Total	MgO/CaO Molar
Q2	3779.2	a	a-2	OD	0.043	0.064	0.126	21.405	0.205	1.019	0	0	35.004	0.022	57.89	0.86
Q2	3779.2	a	a-3	OD	0.121	0.24	0.134	20.681	0.048	0.905	0.045	0.03	35.005	0.005	57.21	0.83
Q2	3779.2	a	a-4	OD	0.133	0.442	0.51	20.281	0.097	1.096	0.033	0.05	34.813	-	57.45	0.82
Q2	3779.2	a	a-5	OD	0.142	0.111	0.165	21.504	0.135	0.823	0.017	-	31.853	0.071	54.82	0.95
Q2	3779.2	a	a-6	OD	0.101	0.423	0.129	18.709	0.079	4.685	0.022	0.035	33.715	0.079	57.98	0.78
Q2	3762.6	b	b-6	CD	0.128	0.236	1.039	21.128	0.123	0.839	0.044	-	34.494	0.079	58.11	0.86
Q2	3762.6	b	b-7	CD	0.142	0.16	0.677	20.456	0.171	0.663	0.027	0.005	34.295	0.061	56.66	0.84
Q2	3779.2	c	c-1	CD	0.133	1.105	0.175	18.799	0.127	1.636	0.075	0.041	32.887	0.029	55.01	0.80
Q2	3779.2	c	c-2	CD	0.129	0.055	0.055	19.3	0.137	4.09	0.021	-	34.984	0.036	58.81	0.77
Q2	3762.6	e	e-2	LD	0.152	0.019	0.046	21.837	0.235	-	0.017	-	32.002	-	54.31	0.96
Q2	3762.6	b	b-8	LD	0.138	0.017	-	23.502	0.212	-	0.006	-	31.674	0.013	55.56	1.04
Q2	3762.6	b	b-9	LD	0.086	0.001	-	22.164	0.161	0.163	0.016	0.052	32.291	0.072	55.01	0.96
Q2	3762.6	f	f-7	LD	0.09	-	0.143	21.32	0.105	0.758	0.005	0.019	34.946	0.054	57.44	0.85
Q2	3762.6	f	f-8	LD	0.126	0.119	0.343	22.183	0.121	0.681	0.028	0.015	33.014	0.048	56.68	0.94
Q2	3779.2	d	d-1	LD	0.094	0.033	-	21.237	0.102	0.364	0.022	0.032	27.644	0.047	49.58	1.08
Q2	3762.6	e	e-1	FD	0.123	0.017	-	19.593	0.048	0.031	0.011	0.052	30.474	0.03	50.38	0.90
Q2	3762.6	f	f-1	FD	0.133	0.019	1.643	21.089	0.112	0.877	0.02	-	33.189	0.04	57.12	0.89
Q2	3762.6	f	f-2	FD	0.105	0.016	0.179	19.137	0.095	0.414	-	-	33.931	0.014	53.89	0.79

Note: OD = dolomite in circular oolitic layers; CD = coating dolomite; LD = pore-lining dolomite; FD = pore-filling dolomite.

## 5. Discussion

### 5.1. Oxygen Isotope Geothermometer

Urey et al. first proposed that the  $^{18}\text{O}$  contents of carbonate rocks could be used to determine the temperature at which they formed, and they applied this concept to the reconstruction of Late Cretaceous paleo-oceanic temperatures in England, Denmark and the Southeastern United States. Many “paleotemperature” equations depend on the  $\delta^{18}\text{O}$  contents of carbonate and water [50–52]. This paper employed the oxygen isotope temperature fractionation equation recommended by Vasconcelos:

$$1000\ln\alpha_{\text{d-w}} = 2.73 \times 10^6 \times T^{-2} + 0.26 \quad (1)$$

where  $\alpha_{\text{d-w}}$  is the oxygen isotope fractionation coefficient between dolomite and water, and  $T$  is the temperature in Kelvin [53]. We chose LD at a depth of 3382.1 m, which has a homogenization temperature of 27.8 °C, for which the  $\delta^{18}\text{O}$  isotopic value was  $-0.76$  based on the laser microsampling technique (Table 1). Therefore, a  $\delta^{18}\text{O}_\text{w}$  of  $-0.7647\text{‰}$  could be calculated using Equation (1). The results are shown in Table 1. The paleotemperatures of the CD ranged from 28.9 to 56.9 °C, whereas those of the LD and FD ranged from 27.8 to 83.1 °C and from 35.6 to 83 °C, respectively. Currently, the boundary between low temperature and high temperature dolomitization in geological environments is still controversial [54,55]. In this paper, we chose 80 °C as the approximate boundary between low temperature and high temperature dolomitization environments. Therefore, most of the dolomitization fluids of E<sub>2s</sub> in the Shijiutuo Uplift area were low temperature dolomitization fluids [55].

### 5.2. Paleoenvironmental Analysis

The carbon and oxygen isotopic compositions of dolomite can be used to analyze whether the lake basin was open or closed and to quantitatively determine the paleosalinity of the sedimentary environment [17,55,56]. In open freshwater lakes, the water remains in the lake for a short time, and the  $\delta^{13}\text{C}$  and  $\delta^{18}\text{O}$  values of the carbonate rocks are both negative; there is no obvious correlation, such as in Hulleh in Israel, Greifensee in Switzerland and Henderson in the United States. In a closed saltwater lake environment, the water is stable, and the  $\delta^{13}\text{C}$  and  $\delta^{18}\text{O}$  values of the carbonate rocks have a significant synchronous correlation; the more strongly the system is sealed, the higher the correlation coefficient, such as in Atlanton-Magadi and Turkana in Africa and the Great Salt Lake in North America (Figure 5). The correlation coefficient of the carbon and oxygen isotopes in the study area is 0.7, indicating that the two are correlated. The drop point falls in the second quadrant, and it is speculated that the lake basin water body of E<sub>2s</sub> in the Shijiutuo area had a certain amount of closure during the sedimentation period; however, the correlation is relatively weak, which indicates that the changes in the carbon and oxygen isotopes are not affected by a single factor [57,58].

Both  $\delta^{18}\text{O}$  and  $\delta^{13}\text{C}$  isotope values are related to salinity, and the variation trend is that the higher the salinity is, the higher the  $\delta$  value is. Keith and Weber (1964) proposed the use of  $Z$  values to distinguish between marine and terrestrial environments [59]. Marine facies are represented by  $Z$  values greater than 120, whereas continental facies have  $Z$  values less than 120. The formula for the  $Z$  value is  $Z = 2.048(\delta^{13}\text{C}_\text{d} + 50) + 0.498(\delta^{18}\text{O}_\text{d} + 50)$ , where  $\delta^{13}\text{C}_\text{d}$  and  $\delta^{18}\text{O}_\text{d}$  are the isotopic compositions of dolomite (VPDB). The results show that most of the dolomite samples have  $Z$  values of  $>125$ , which indicates that these dolomites formed in a high-salinity saltwater environment. Based on the salinity formula  $S = \delta^{18}\text{O}_\text{d} + 21.2/0.61$  (where  $\delta^{18}\text{O}_\text{d}$  is the isotopic composition of dolomite), the average salinity of the study area is 29.7‰ (Table 1), which represents a saltwater lake [58]. The high salinity characteristics are mainly caused by two factors. First, the paleoclimate was relatively hot at the time of sedimentation of E<sub>2s</sub>, the lake water was relatively closed, and the evaporation was intense, resulting in less lake water input than evaporation. Second, it is speculated that E<sub>2s</sub> in the study area was affected by seawater invasion, and the intrusion of high salinity seawater increased the

salinity of the lake water [58,60,61]. In the relatively closed ancient environment, the small influence of surface runoff and the high salinity of the water body may explain the high  $\delta^{18}\text{O}$  values relative to typical lacustrine carbonate rocks.

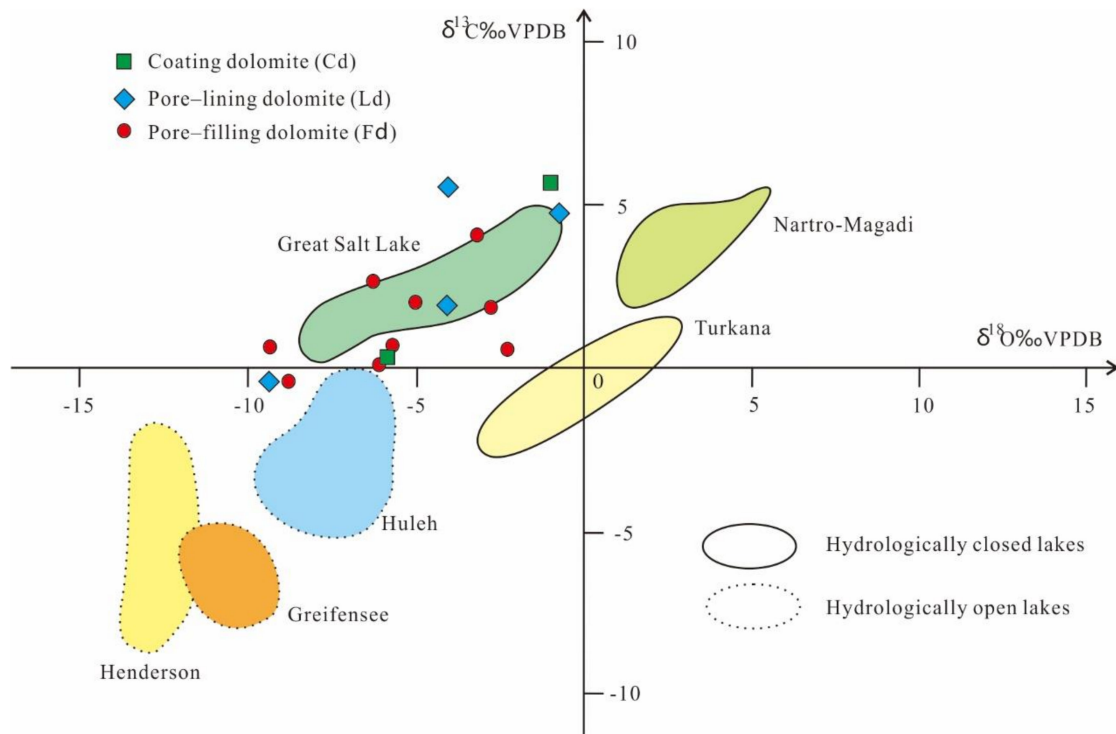


**Figure 5.** Carbon and oxygen isotopic compositions of different types of dolomite and sedimentary environments of the Paleogene Shahejie Formation in the Shijiutuo area, Bohai area [17,55,56].

### 5.3. Genetic Analysis of Authigenic Dolomite

Dolomites form under different conditions and in different depositional environments [51]. Despite decades of intense study, it is still difficult to provide an unequivocal genetic interpretation that traces the complete depositional and burial evolution of a dolomite [25]. It is generally agreed that any dolomitization model must (1) explain the supply of  $\text{Mg}^{2+}$  and (2) provide a delivery mechanism (e.g., hydrological and thermodynamic conditions) [62,63].

#### 5.3.1. Source of $\text{Mg}^{2+}$

##### $\text{Mg}^{2+}$ in Pulverite

The elemental analysis showed that the mudstone in E<sub>2</sub>S contained high proportions of MgO, with an average content of 2.07%, which is similar to the MgO contents of mudstones in typical salt lakes [38,64–69]. The mean value of  $\text{Mg}^{2+}/\text{Ca}^{2+}$  (mol) is 2.1, which is much larger than that of standard stoichiometric dolomite and indicates that this mudstone is Mg-rich (Table 2). A large amount of  $\text{Mg}^{2+}$  can be released from mudstones into the pore fluid during burial by various processes, such as hydration, compaction, and dehydration, which provide the essential material conditions for the formation of dolomite during diagenesis [56,70–73].

##### $\text{Mg}^{2+}$ in Intraclasts

E<sub>2</sub>S contains abundant carbonate intraclasts and bioclots. As indicated by the compositional analysis of various cortical laminae of oolites, the MgO contents exhibited certain evolutionary characteristics (Figure 6a). The MgO contents were higher in the inner layers than in the outermost

layers, indicating that Mg was enriched in the sedimentary fluid during the early stages. With the continuous depletion of Mg caused by the oolitic circle formation, the MgO contents in the outermost circular layers decreased. The FeO contents were lower in the early-stage circular layers and higher in the outermost circular layers (Figure 6b), which also indicates that the environment changed from an oxidative environment to a reductive environment.

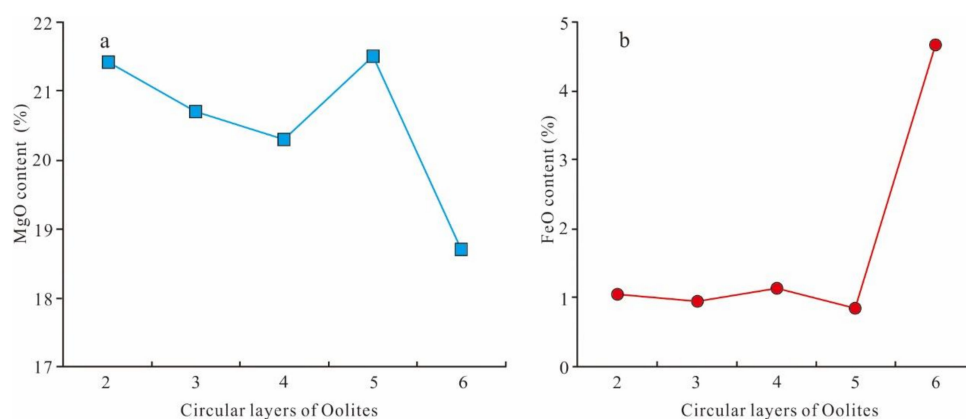


**Figure 6.** MgO and FeO contents in different circular layers of oolites.

### Mg<sup>2+</sup> from Seawater Invasion

The concentration of Mg<sup>2+</sup> in seawater is much higher than that in lake water and the salinity index Z value of dolomite in the study area is greater than 120, which indicates the possibility that seawater may have entered the lake basin periodically during the sedimentation of E<sub>2</sub>s, which led to the increasing salinity of the lake basin water. In addition, previous studies have found that Sr/Ba values of E<sub>2</sub>s in several depressions of Bohai Bay Basin were greater than 1 [58,60,61], indicating that the study area may be affected by transgression.

### 5.3.2. Delivery Mechanism

The fluid driving force is another key factor for dolomite formation [62,63]. The driving force of Mg<sup>2+</sup> fluid in the study area mainly had the following two mechanisms. First, heavy saltwater formed on the surface of the lake by evaporation and moved to the bottom of the lake due to the effect of density [55,74,75]. Second, on the edge of the lake basin or in the uplifted region of grain beach facies, the highly concentrated brine was affected by gravity flows along the slopes on either side of the ancient uplift [18,19].

### 5.3.3. Model for the Origin of Authigenic Dolomite

The temperature dependence on the oxygen isotope geothermometers indicated that the formation temperatures of the authigenic dolomite had a slightly broad range (from 27.8 to 83.1 °C). The sedimentary paleogeomorphology and rock mineral characteristics indicate that the lacustrine dolomite in E<sub>2</sub>s in the Shijiutuo Uplift formed in two stages. The first stage was the reflux and infiltration of brine. Due to the evaporation of lake water, seawater invasion, and the compaction and dehydration of fine sediments, the concentration of Mg<sup>2+</sup> in the lake water increased significantly. This Mg<sup>2+</sup>-rich lake water flowed to the lake bottom due to density and gravity. The lake-bottom water had poor circulation, which resulted in a reducing environment and high-salinity alkaline water conditions. Dolomitization occurred when heavy brine penetrated further into the larger limestone layers. Because of the rapid nucleation and crystallization of the dolomite that formed in this environment, very fine crystals of CD or early LD formed. The second stage was the adjustment stage of burial. With increasing burial depth and the reduction environment, the Fe<sup>2+</sup> content in the dolomite increased (Figure 6b). In addition, early dolomite adjusted and enhanced the dolomitization to form larger crystal LD or FD.

#### 5.4. Geological Significance

A large number of studies have confirmed that carbonate cements have a significant impact on reservoir quality and are generally considered to be negative [76–79]. Recent evidence has shown that carbonate cements have two competing influences on the physical properties of reservoirs—they occupy pore space but also help to resist compaction [9,80,81].

The petrographic analysis, cathodoluminescence analysis, and oxygen isotope characteristics described above indicated that the authigenic dolomites in the study area mainly formed in the early diagenetic stage. The microscopy observations revealed that most of the LD grew around the intergranular pores and did not develop in the areas in which the particles came into contact. However, the presence of CD-covered particles indicated that it grew before the particles were in contact with each other, which means that the CD may be penecontemporaneous dolomite. The CD crystals were mainly very fine crystals that were smaller than the LD crystals (Figure 2a,b). This finding indicated that the CD formed during the same period as the early LD or before it. The cathodoluminescence of the CD was faint (Figure 3a,b), which indicated that it had not experienced strong diagenetic alteration and formed during early diagenesis. The LD with a blade-like or overhanging appearance may represent the formation of this cement in the vadose zone [82]. According to oxygen isotope geothermometers, most of the dolomitization fluids in E<sub>2</sub>s in the Shijiutuo Uplift area were low temperature dolomitization fluids. During this early diagenetic stage, the microcrystalline CD developed around particles, the early lining dolomite precipitated in the intergranular pores, and the Mg content of the dolomitization fluids decreased continuously. Once the dolomitization fluids had exhausted their Mg, they continued to flow basin-ward without causing further dolomitization. If sufficient Mg<sup>2+</sup> remained in the pore fluid, it would form FD or late LD (i.e., second-generation or third-generation LD) (Figure 7) [55,83]. The coating and early-stage LD (first-generation lining) developed during early diagenesis, thus allowing the grains to support each other and to resist further mechanical compaction. However, the late-stage LD (second- or third-generation lining) and the FD mainly caused a significant decrease in porosity by filling the interparticle pores and moldic pores. Therefore, the carbonate cements that formed in the early stage of diagenesis played a positive role in the physical properties of the reservoir, whereas the carbonate cements that formed in the late stages of diagenesis played a negative role [84,85]. However, further work is needed to quantify the effects of the different types of cements on the quality of the reservoir.

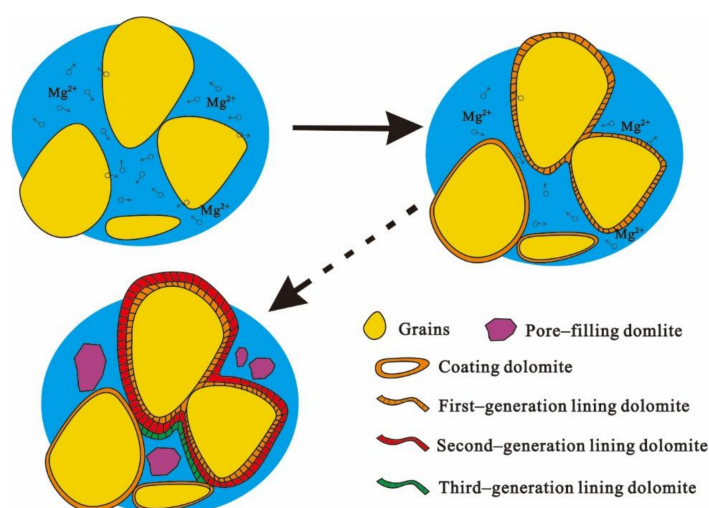


**Figure 7.** Origin of dolomite showing that with the consumption of Mg<sup>2+</sup>, the microcrystalline coating dolomite and the early lining dolomite precipitate formed. If sufficient Mg<sup>2+</sup> remained in the diagenetic fluid, pore-filling dolomite or late lining dolomite will be formed.

## 6. Conclusions

The carbon isotopic compositions of different types of dolomite cements in E<sub>2</sub>s in the Shijiutuo Horst area mostly range from −2‰ to 6‰, which conforms to the characteristics of typical lacustrine carbonate rocks. However, the oxygen isotope compositions have an obvious positive deviation. The relatively closed paleoenvironment, the small influence of surface runoff, and the high salinity of the water body may explain the high δ<sup>18</sup>O values relative to typical lacustrine carbonate rocks. The sedimentary environment of E<sub>2</sub>s in the study area was a relatively closed lake environment with high salinity. As a result, the diagenetic fluids were rich in Mg<sup>2+</sup> (due to the evaporation of lake water, seawater invasion, and the compaction and dehydration of fine sediments), which is necessary for the formation of authigenic dolomite.

The dolomite cements in the study area may have experienced two stages of dolomitization: seepage-reflux dolomitization during the penecontemporaneous period and burial dolomitization. The CD and LD formed in the early stage of diagenesis, which may have enhanced the strength of these rocks and played a positive role in the reservoir's physical properties.

**Author Contributions:** Conceptualization, H.M., Z.L. and Z.S.; Data curation, H.M. and C.X.; Investigation, Z.S.; Methodology, Z.L.; Software, C.X.; Supervision, Z.L.; Writing—original draft, H.M.; Writing—review and editing, H.M., Z.L. and Z.S. **Funding** This work was financially supported by the National Science & Technology Specific Project (Grant No. 2011ZX05023-006).

**Conflicts of Interest:** The authors declare that they have no conflicts of interest to disclose.

## References

1. Bath, A.; Milodowski, A.; Spiro, B. Diagenesis of carbonate cements in Permo-Triassic sandstones in the Wessex and East Yorkshire-Lincolnshire Basins, UK: A stable isotope study. *Geol. Soc. Lond. Spec. Publ.* **1987**, *36*, 173–190. [[CrossRef](#)]
2. Munawar, M.J.; Lin, C.; Dong, C.; Zhang, X.; Zhao, H.; Azeem, T.; Zahid, M.A.; Ma, C. Architecture and reservoir quality of low-permeable Eocene lacustrine turbidite sandstone from the Dongying Depression, East China. *Open Geosci.* **2018**, *10*, 87–112. [[CrossRef](#)]
3. Chowdhury, A.H.; Noble, J.P.A. Origin, distribution and significance of carbonate cements in the Albert Formation reservoir sandstones, New Brunswick, Canada. *Mar. Pet. Geol.* **1996**, *13*, 837–846. [[CrossRef](#)]
4. Dutton, S.P.; Flanders, W.A. Evidence of reservoir compartmentalization by calcite cement layers in deepwater sandstones, Bell Canyon Formation, Delaware Basin, Texas. *Geol. Soc. Lond. Spec. Publ.* **2004**, *237*, 279–282. [[CrossRef](#)]
5. Dutton, S.P. Calcite cement in Permian deep-water sandstones, Delaware Basin, west Texas: Origin, distribution, and effect on reservoir properties. *AAPG Bull.* **2008**, *92*, 765–787. [[CrossRef](#)]
6. Taylor, T.R.; Giles, M.R.; Hathon, L.A.; Diggs, T.N.; Braunsdorf, N.R.; Birbiglia, G.V.; Kittridge, M.G.; Macaulay, C.I.; Espejo, I.S. Sandstone diagenesis and reservoir quality prediction: Models, myths, and reality. *AAPG Bull.* **2010**, *94*, 1093–1132. [[CrossRef](#)]
7. Shen, J.; Chen, B.; Chen, F.; Cheng, C.; Li, Y.; Tian, Y. Paleogene lacustrine dolomitization, Xingou region, southern Qianjiang Depression, China. *Geosci. J.* **2016**, *20*, 183–197. [[CrossRef](#)]
8. Wang, J.; Cao, Y.; Liu, K.; Liu, J.; Xue, X.; Xu, Q. Pore fluid evolution, distribution and water-rock interactions of carbonate cements in red-bed sandstone reservoirs in the Dongying Depression, China. *Mar. Pet. Geol.* **2016**, *72*, 279–294. [[CrossRef](#)]
9. Xiong, D.; Azmy, K.; Blamey, N.J.F. Diagenesis and origin of calcite cement in the Flemish Pass Basin sandstone reservoir (Upper Jurassic): Implications for porosity development. *Mar. Pet. Geol.* **2016**, *70*, 93–118. [[CrossRef](#)]
10. Bustillo, M.A.; Armenteros, I.; Huerta, P. Dolomitization, gypsum calcitization and silicification in carbonate-evaporite shallow lacustrine deposits. *Sedimentology* **2017**, *64*, 1147–1172. [[CrossRef](#)]
11. Cui, Y.; Jones, S.J.; Saville, C.; Stricker, S.; Wang, G.; Tang, L. The role played by carbonate cementation in controlling reservoir quality of the Triassic Skagerrak Formation, Norway. *Mar. Pet. Geol.* **2017**, *85*, 316–331. [[CrossRef](#)]

12. Cui, Y.; Wang, G.; Jones, S.J.; Zhou, Z.; Ran, Y.; Lai, J.; Li, R. Prediction of diagenetic facies using well logs—A case study from the Upper Triassic Yanchang Formation, Ordos Basin, China. *Mar. Pet. Geol.* **2017**, *81*, 50–65. [[CrossRef](#)]
13. Yang, Y.; Qiu, L.; Gregg, J.M.; Puckette, J.; Liu, K. Characterization of lacustrine carbonate reservoirs in the eocene Sikou Sag, Bohai Bay Basin, East China. *Carbonates Evaporites* **2017**, *32*, 75–93. [[CrossRef](#)]
14. Tutolo, B.M.; Tosca, N.J. Experimental examination of the mg-silicate-carbonate system at ambient temperature: Implications for alkaline chemical sedimentation and lacustrine carbonate formation. *Geochim. Cosmochim. Acta* **2018**, *225*, 80–101. [[CrossRef](#)]
15. Zhang, G. An evaluation of exploration potential in Bodong area from the major discovery of shallow oil and gas in Shijiutuo Uplift. *China Offshore Oil Gas* **2000**, *14*, 84–92, (In Chinese with English abstract).
16. Wang, Y.; Xue, Y.; Wang, G.; Li, G. Shallow layer hydrocarbon accumulation characteristics and their exploration significances in Shijiutuo Uplift, Bohai Sea. *China Offshore Oil Gas* **2015**, *27*, 8–16, (In Chinese with English Abstract).
17. Pan, W.; Wang, Q.; Liu, S.; Feng, C.; Tian, D. Origin of lacustrine bioclastic dolostone in the Paleogene Shahejie Formation: A case study in Shijiutuo area, Bohai Sea. *J. Palaeogeogr.* **2017**, *19*, 835–848.
18. Shi, W.; Li, H.; Mao, L.; Yang, H.; Chen, L.; Yu, H. Hydrocarbon Geological Characteristics and Exploration Potential of Qinnan Depression in Offshore Area of Bohai Sea. *China Pet. Explor.* **2014**, *19*, 32–40.
19. Lv, Z.X.; Song, X.Z.; Qing, Y.; Qi, Y.; Jin, X. Characteristics of deep and high-quality Paleogene lacustrine carbonate reservoir in central Bohai Sea. *Nat. Gas Ind.* **2015**, *36*, 10–17, (In Chinese with English Abstract).
20. Melim, L.A.; Swart, P.K.; Eberli, G.P. Mixing-zone Diagenesis in the subsurface of Florida and the Bahamas. *J. Sediment. Res.* **2004**, *74*, 904–913. [[CrossRef](#)]
21. Ma, Y.; Guo, X.; Guo, T.; Huang, R.; Cai, X.; Li, G. The puguang gas field: New giant discovery in the mature Sichuan Basin, southwest China. *AAPG Bull.* **2007**, *91*, 627–643. [[CrossRef](#)]
22. Breesch, L.; Swennen, R.; Vincent, B.; Ellison, R.; Dewever, B. Dolomite cementation and recrystallisation of sedimentary breccias along the Musandam Platform margin (United Arab Emirates). *J. Geochem. Explor.* **2010**, *106*, 34–43. [[CrossRef](#)]
23. Iannace, A.; Frijia, G.; Galluccio, L.; Parente, M. Facies and early dolomitization in Upper Albian shallow-water carbonates of the southern Apennines (Italy): Paleotectonic and paleoclimatic implications. *Facies* **2014**, *60*, 169–194. [[CrossRef](#)]
24. Li, M.; Lin, X.; Tian, J.C.; Peng, S.F.; Xu, L.; Su, L. Study on variously dolomitized reservoir reef at platform margin of Changxing Formation in northeastern Sichuan Basin, southwestern China. *Carbonates Evaporites* **2018**, *6*, 1–14.
25. Warren, J. Dolomite: Occurrence, evolution and economically important associations. *Earth Sci. Rev.* **2000**, *52*, 1–81. [[CrossRef](#)]
26. Zhao, W.Z.; Shen, A.J.; Zheng, J.F.; Qiao, Z.F.; Wang, X.F.; Lu, J.M. The porosity origin of dolostone reservoirs in the Tarim, Sichuan and Ordos basins and its implication to reservoir prediction. *Sci. China Earth Sci.* **2014**, *57*, 2498–2511. [[CrossRef](#)]
27. Mariusz, P.; Andrzej, P.; Karina, A.; Aleksandra, P.; Marcin, S. The significance of Chara vegetation in the precipitation of lacustrine calcium carbonate. *Sedimentology* **2013**, *60*, 1017–1035.
28. Grotzinger, J.; Al-Rawahi, Z. Depositional facies and platform architecture of microbialite-dominated carbonate reservoirs, Ediacaran-Cambrian Ara Group, Sultante of Om. *Am. Assoc. Pet. Geol.* **2014**, *98*, 1453–1494. [[CrossRef](#)]
29. Chagas, A.A.P.; Webb, G.E.; Burne, R.V.; Southam, G. Modern lacustrine microbialites: Towards a synthesis of aqueous and carbonate geochemistry and mineralogy. *Earth Sci. Rev.* **2016**, *162*, 338–363. [[CrossRef](#)]
30. Qing, H.R.; Mountjoy, E.W. Formation of coarsely crystalline, hydrothermal dolomite reservoirs in the Presquile Barrier, western Canada Sedimentary Basin. *Am. Assoc. AAPG Bull.* **1994**, *78*, 55–77.
31. Hollis, C.; Bastesen, E.; Boyce, A.; Corlett, H.; Gawthorpe, R.; Hirani, J.; Rotevatn, A.; Whitaker, F. Fault-controlled dolomitization in a rift basin. *Geology* **2017**, *45*, 219–222. [[CrossRef](#)]
32. Jiang, L.; Worden, R.H.; Yang, C. Thermochemical sulphate reduction can improve carbonate petroleum reservoir quality. *Geochim. Cosmochim. Acta* **2018**, *223*, 127–140. [[CrossRef](#)]
33. Al-Aasm, I.; Lonnee, J.; Clarke, J. Multiple fluid flow events and the formation of saddle dolomite: Examples from middle Devonian carbonates of the western Canada Sedimentary Basin. *J. Geochem. Explor.* **2000**, *69–70*, 11–15. [[CrossRef](#)]

34. Feng, M.; Wu, P.; Qiang, Z. Hydrothermal dolomite reservoir in the Precambrian Dengying Formation of central Sichuan Basin, southwestern China. *Mar. Pet. Geol.* **2017**, *82*, 206–219. [[CrossRef](#)]
35. Liu, Z.; Zhou, X.; Li, J.; Lai, W. Reservoir characteristics and controlling factors of the paleogene Sha-2 member in 36-3 structure, eastern Shijiutuo Uplift, Bohai Sea. *Oil Gas Geol.* **2011**, *32*, 832–838, (In Chinese with English Abstract).
36. Qing, Y.H.; Lv, Z.X.; Wang, X.D.; Song, X.Z.; Zhang, S.L.; Meng, H.L. Porosity evolution of high-quality reservoirs in deep palaeogene lacustrine carbonate rocks in the central bohai sea. *Energy Explor. Exploit.* **2018**, in press. [[CrossRef](#)]
37. Ni, J.; Sun, L.; Li, G.; He, J.; Zhao, W.; Liu, X. Depositional patterns of the 2nd member of the Shahejie Formation in Q oilfield of the Shijiutuo Uplift, Bohai Sea. *Oil Gas Geol.* **2013**, *34*, 491–498, (In Chinese with English Abstract).
38. Peng, L. Heterogeneity and Controlling Factors of Lithofacies of the Lower 3rd Member of Paleogene Shahejie Formation Lacustrine Shale in Jiyang Depression. Ph.D. Thesis, China University of Geosciences, Beijing, China, 2017. (In Chinese with English Abstract).
39. Zhang, Y.; Hu, X.; Tao, N.; Zhang, X.; Gao, Y.; Hui, W.; Fan, T.; Bu, F. Controlling of Paleogeomorphology to Paleogene Sedimentary System of Shijiutuo Uplift in Bohai Basin. *J. Jilin Univ.* **2015**, *45*, 1590–1596.
40. Li, J.P.; Zhou, X.H. On the distribution of the kongdian formation in the Bohai area with special reference to its bearings on oil exploration. *J. Stratigr.* **2010**, *34*, 89–96.
41. Wang, Q.M.; Du, X.F.; Jia, D.H.; Wan, L.W. The 1st and 2nd members of the Shahejie Formation in No.428 uplifted area, Bohai Sea: Sedimentary systems and their controlling factors. *Sedim. Geol. Tethyan Geol.* **2015**, *35*, 12–16.
42. Zhang, Y.; Wang, H.; Hu, X.; Zhang, X.; Bu, F.; Gao, Y. Reservoir modeling of complex lithologies with sparse wells: A case from a oilfield in Shijiutuo uplift, Bohai Bay Basin. *Oil Gas Geol.* **2016**, *37*, 450–456, (In Chinese with English Abstract).
43. Yu, H.Z.; Wang, Y.; Jiang, T.; Chuai, Y.; Yang, H. Discovery of Bioclastic Dolostone in the Second Member of Shahejie Formation in Bozhong Depression and Its Significance in Oil Exploration. *Sci. Technol. Rev.* **2010**, *28*, 60–64.
44. Lv, Z.X.; Zhang, S.L.; Yin, C.; Meng, H.L. Features and genesis of Paleogene high-quality reservoirs in lacustrine mixed siliciclastic-carbonate sediments, central Bohai Sea, China. *Pet. Sci.* **2017**, *14*, 50–60.
45. Blamey, N.J.F.; Azmy, K.; Brand, U. Provenance and burial history of cement in sandstones of the Northbrook Formation (Carboniferous), western Newfoundland, Canada: A geochemical investigation. *Sediment. Geol.* **2014**, *299*, 30–41. [[CrossRef](#)]
46. Lindholm, R.C.; Finkelman, R.B. Calcite staining, semiquantitative determination of ferrous iron. *J. Sediment. Res.* **1972**, *42*, 239–242. [[CrossRef](#)]
47. Luo, P.; Su, L.P.; Luo, Z. Application of laser micro-sampling technique to analysis of C and O isotopes of oolitic dolomites in Feixianguan Formation. *Northeast Sichuan Geochim.* **2006**, *35*, 325–330.
48. Kelts, K.; Talbot, M. *Lacustrine Carbonates as Geochemical Archives of Environmental Change and Biotic/Abiotic Interactions*; Springer: Berlin/Heidelberg, Germany, 1990; pp. 288–315.
49. Pan, L.Y.; Huang, G.P.; Shou, J.F.; Liu, Z.G. A Preliminary Study of Formation Environment of the Neogene Lacustrine Carbonates in Nanyishan Area of Qaidam Basin: Constrains from Carbon-Oxygen Isotope and Fluid Inclusion Analysis. *Bull. Mineral. Petrol. Geochem.* **2009**, *28*, 71–74.
50. Urey, H.C.; Lowenstam, H.A.; Epstein, S.; Mckinney, C.R. Measurement of paleotemperatures and temperatures of the upper cretaceous of England, Denmark, and the southeastern United States. *Geol. Soc. Am. Bull.* **1951**, *62*, 399–416. [[CrossRef](#)]
51. Qing, H. Petrography and geochemistry of early-stage, fine- and medium-crystalline dolomites in the Middle Devonian Presqu'île Barrier at Pine Point, Canada. *Sedimentology* **1998**, *45*, 433–446. [[CrossRef](#)]
52. Matthews, A.; Katz, A. Oxygen isotope fractionation during the dolomitization of calcium carbonate. *Geochim. Cosmochim. Acta* **1977**, *41*, 1431–1438. [[CrossRef](#)]
53. Vasconcelos, C.; Mckenzie, J.A.; Warthmann, R.; Bernasconi, S.M. Calibration of the  $\delta^{18}\text{O}$  paleothermometer for dolomite precipitated in microbial cultures and natural environments. *Geology* **2005**, *33*, 317–320. [[CrossRef](#)]
54. Lovering, T.S. The origin of hydrothermal and low temperature dolomite. *Econ. Geol.* **1969**, *64*, 743–754. [[CrossRef](#)]

55. Machel, H.G. Concepts and models of dolomitization: A critical reappraisal. *Geol. Soc. Lond. Spec. Publ.* **2004**, *235*, 7–63. [[CrossRef](#)]
56. Talbot, M.R. A review of the palaeohydrological interpretation of carbon and oxygen isotopic ratios in primary lacustrine carbonates. *Chem. Geol. Isotope Geosci.* **1990**, *8*, 261–279. [[CrossRef](#)]
57. Yuan, J.Y.; Huang, C.G.; Cao, Z.L.; Li, Z.Y.; Wan, C. Carbon and oxygen isotopic composition of saline lacustrine dolomite and its palaeoenvironmental significance: A case study of Lower Eocene Ganchaigou Formation in western Qaidam Basin. *Geochimica* **2015**, *44*, 48–54.
58. Wang, B.J.; Cai, M.J.; Lin, C.M.; Zhang, X. Characteristics and origin of lacustrine dolostone of the Paleogene Shahejie Formation in Tanggu area, Bohai Bay Basin. *J. Palaeogeogr.* **2014**, *16*, 65–76.
59. Keith, M.L.; Weber, J.N. Carbon and oxygen isotopic composition of selected limestones and fossils. *Geochim. Cosmochim. Acta* **1964**, *28*, 1787–1816. [[CrossRef](#)]
60. Wang, G.M.; Zhong, J.H.; Jiang, Z.X. Possible transgressive channel in paleogene deduced by lateral change of palaeosalinity in 1st Member of Shahejie Formation in Jiyang Depression. *World Geol.* **2005**, *24*, 243–247.
61. Yuan, W.F.; Zeng, C.M.; Chen, S.Y. Characteristic of dinosterane and C<sub>31</sub> Sterane in Paleocene Saline Formation of Jiyang Depression. *Acta Sedimentol. Sin.* **2008**, *26*, 683–687.
62. Morrow, D.W. Diagenesis, 2. Dolomite—Part 2-dolomitization models and ancient dolostones. *Research* **1982**, *9*, 95–107.
63. Zhao, H.W.; Brian, J. Genesis of fabric-destructive dolostones: A case study of the Brac Formation (Oligocene), Cayman Brac, British West Indies. *Sediment. Geol.* **2012**, *267–268*, 36–54. [[CrossRef](#)]
64. Braitsch, O. *Salt Deposits Their Origin and Composition*; Springer: Berlin/Heidelberg, Germany, 1971.
65. Carroll, D. Clay minerals: A guide to their X-ray identification. *Spec. Pap. Geol. Soc. Am.* **1970**, *126*, 1–80.
66. Darby, D.A. Kaolinite and other clay minerals in Arctic Ocean sediments. *J. Sediment. Petrol.* **1975**, *45*, 272–279.
67. Degens, E.T. *Geochemistry of Sediments: A Brief Survey*; Prentice-Hall: Upper Saddle River, NJ, USA, 1965.
68. Xu, C. Preliminary research on clay minerals in salt lake sediments of china and its significance. *Sci. China Chem.* **1991**, *34*, 490–501.
69. Xuan, Z. Review for the 50-years History of the Chinese Potassium Salts and the Prospects. *J. Salt Lake Res.* **2000**, *8*, 58–62.
70. Jodry, R.L. Growth and Dolomitization of Silurian Reefs, St. Clair County, Michigan. *AAPG Bull.* **1969**, *53*, 957–981.
71. Machel, H.G.; Anderson, J.H. Pervasive subsurface dolomitization of the Nisku Formation in central Alberta. *J. Sediment. Petrol.* **1989**, *59*, 891–911.
72. Garven, G.; Freeze, R. Theoretical analysis of the role of groundwater flow in the genesis of stratabound ore deposits. *Am. J. Sci.* **1984**, *284*, 1085–1174. [[CrossRef](#)]
73. Folk, R.L. Mg/Ca ratio and salinity: Two controls over crystallization of dolomite. *AAPG Bull.* **1975**, *59*, 60–68.
74. Huang, C.G.; Yuan, J.Y.; Wu, L.Y. Origin and research methods of lacustrine dolomite. *Lithol. Reserv.* **2016**, *28*, 7–15, (In Chinese with English Abstract).
75. Bjørlykke, K. Relationships between depositional environments, burial history and rock properties. Some principal aspects of diagenetic process in sedimentary basins. *Sediment. Geol.* **2014**, *301*, 1–14. [[CrossRef](#)]
76. Rossi, C.; Marfil, R.; Ramseyer, K. Facies-Related Diagenesis and Multiphase Siderite Cementation and Dissolution in the Reservoir Sandstones of the Khatatba Formation, Egypt's Western Desert. *J. Sediment. Res.* **2001**, *71*, 459–472. [[CrossRef](#)]
77. Kantorowicz, J.D.; Bryant, I.D.; Dawans, J.M. Controls on the geometry and distribution of carbonate cements in Jurassic sandstones: Bridport Sands, southern England and Viking Group, Troll Field, Norway. *Geol. Soc. Lond. Spec. Publ.* **1987**, *36*, 103–118. [[CrossRef](#)]
78. Hu, Z.Q. Calcite cements in Upper Palaeozoic sand reservoir of Ordos Basin. *Acta Pet. Sin.* **2003**, *24*, 40–43, (In Chinese with English Abstract).
79. Liu, C.Y.; Zheng, H.R.; Hu, Z.Q. Characteristics of carbonate cementation in clastic rocks from the Chang 6 sandbody of Yanchang Formation, southern Ordos Basin. *Sci. China Earth Sci.* **2012**, *55*, 58–66. [[CrossRef](#)]
80. Chen, B.; Liu, Y.; Liu, H. Reservoir characteristics and evaluation of the Permian Xiazijie Formation in Wuerhe area, Junggar Basin. *Lithol. Reserv.* **2015**, *27*, 53–60.

81. Wei, W.; Zhu, X.M.; Guo, D.B. Carbonate cements in Lower Cretaceous Bayingebi sandstone reservoirs in Chagan Sag, Yin-e Basin: Formation phases and formation mechanisms. *Geochimica* **2015**, *44*, 590–599, (In Chinese with English Abstract).
82. Flügel, E. *Microfacies of Carbonate Rocks*; Springer: Berlin/Heidelberg, Germany, 2004; pp. 267–334.
83. Saller, A.H.; Henderson, N. Distribution of Porosity and Permeability in Platform Dolomites: Insight from the Permian of West Texas: Reply. *AAPG Bull.* **2001**, *82*, 1528–1550.
84. Sun, S.Q. Dolomite reservoirs: Porosity evolution and reservoir characteristics. *AAPG Bull.* **1995**, *79*, 186–204.
85. Jiang, L.; Cai, C.; Worden, R.H.; Crowley, S.F.; Jia, L.; Zhang, K.; Duncan, I.J. Multiphase dolomitization of deeply buried Cambrian petroleum reservoirs, Tarim Basin, north–west China. *Sedimentology* **2016**, *63*, 2130–2157. [[CrossRef](#)]



© 2018 by the authors. Licensee MDPI, Basel, Switzerland. This article is an open access article distributed under the terms and conditions of the Creative Commons Attribution (CC BY) license (<http://creativecommons.org/licenses/by/4.0/>).